CLIMATOLOGY

On the glacial-interglacial variability of the Asian monsoon in speleothem $\delta^{18}O$ records

G. Liu[1,2,3]*, X. Li[4], H.-W. Chiang[2], H. Cheng[4], S. Yuan[1,2,3], S. Chawchai[5], S. He[2], Y. Lu[2], L. T. Aung[2,6], P. M. Maung[2,7], W. N. Tun[6], K. M. Oo[7], X. Wang[2,3]*

While Asian monsoon (AM) changes have been clearly captured in Chinese speleothem oxygen isotope ($\delta^{18}O$) records, the lack of glacial-interglacial variability in the records remains puzzling. Here, we report speleothem $\delta^{18}O$ records from three locations along the trajectory of the Indian summer monsoon (ISM), a major branch of the AM, and characterize AM rainfall over the past 180,000 years. We have found that the records close to the monsoon moisture source show large glacial-interglacial variability, which then decreases landward. These changes likely reflect a stronger oxygen isotope fractionation associated with progressive rainout of AM moisture during glacial periods, possibly due to a larger temperature gradient and suppressed plant transpiration. We term this effect, which counteracts the forcing of glacial boundary conditions, the moisture transport pathway effect.

INTRODUCTION

The Asian monsoon (AM) affects the livelihoods of about half the global population. The AM variabilities have been widely inferred on the basis of oxygen isotope ratios ($\delta^{18}O$) in cave records, in particular those from Hulu, Sanbao, and Dongge caves in southern China, which all show $\delta^{18}O$ changed markedly on orbital time scales largely in response to the Northern Hemisphere summer insolation (NHSI), and abruptly on millennial time scales in close correspondence with North Atlantic climate events (*1*, *2*). The Chinese cave records, unlike other monsoon proxy data (*3*–*5*) and global-scale paleoclimate records (*6*–*9*), are insensitive to global ice volume forcing, especially when considering their unexpectedly low $\delta^{18}O$ values during the Last Glacial Maximum [LGM; ~23 to 19 thousand years before present (ka B.P.; B.P. refers to 1950 A.D.) (*10*)] and relatively high $\delta^{18}O$ values during marine isotope stage 5e (MIS 5e) (Fig. 1) (*1*, *2*).

This inconsistency has led to other interpretations, which instead suggest that the $\delta^{18}O$ records either reflect changes in the remote moisture source over the Indian Ocean (the so-called upstream depletion mechanism) (*11*–*13*) or are a result of changing proportions of less ^{18}O-depleted moisture from the western Pacific that is mixed with moisture from the Indian Ocean (*2*, *4*, *14*, *15*). To weigh in on the controversy, here we investigate cave $\delta^{18}O$ with a broader spatial coverage and report its changes over mainland Southeast Asia. Our records are based on stalagmites from three locations: southeastern Myanmar and western Thailand near the eastern coastal Bay of Bengal (CBoB), the western Shan Plateau in central Myanmar (CM), and southeastern Yunnan (SEY), China, close to the Myanmar-China border (Fig. 2 and figs. S1 and S2). These three locations form a SW-NE (southwest-northeast) transect along the moisture trajectory of the Indian summer monsoon (ISM), a major branch of the AM (*16*, *17*).

[1]Interdisciplinary Graduate School, Nanyang Technological University, 639798 Singapore. [2]Earth Observatory of Singapore, Nanyang Technological University, 639798 Singapore. [3]Asian School of the Environment, Nanyang Technological University, 639798 Singapore. [4]Institute of Global Environmental Change, Xi'an Jiaotong University, Xi'an 710049, China. [5]Department of Geology, Chulalongkorn University, Bangkok 10330, Thailand. [6]Myanmar Earthquake Committee, Yangon 11052, Myanmar. [7]Department of Meteorology and Hydrology, Nay Pyi Taw 15011, Myanmar.
*Corresponding author. Email: gxliu@ntu.edu.sg (G.L.); xianfeng.wang@ntu.edu.sg (X.W.)

RESULTS

In total, for this study, we analyzed 19 stalagmites (fig. S3) from 11 caves (see Materials and Methods and table S1); we determined 164 dates using recently improved uranium/thorium dating techniques and constructed the chronologies of all samples (fig. S4) (*18*, *19*); and we measured 2611 stable isotope values (figs. S5 and S6). The records from CBoB (fig. S7A) and CM (fig. S7B) cover a substantial part of the last 40 ka, including both the LGM and the most recent several hundred years. The spliced record from SEY extends almost continuously through the last 180 ka (fig. S7C).

Our three speleothem $\delta^{18}O$ records (fig. S7) broadly resemble the NHSI on orbital time scales, with more negative $\delta^{18}O$ values corresponding to higher insolation and vice versa. The records are also punctuated by abrupt $\delta^{18}O$-positive shifts corresponding to the Younger Dryas and Heinrich event 1. However, the earlier millennial-scale events are less clearly shown, in part due to the coarse resolution of the records.

On glacial-interglacial time scales, our records show relatively more positive values during the glacial periods and more negative values during interglacial periods. For example, the CBoB $\delta^{18}O$ (fig. S7A) was ~−3 to ~−6‰ between ~18 and ~37 ka, but about −7.5‰ during the recent few hundred years. Similarly, the CM record (fig. S7B) presents $\delta^{18}O$ values ~−5‰ to ~−7‰ and ~−7.5‰ during the late glacial and late Holocene, respectively. The SEY record (fig. S7C) shows relatively more positive $\delta^{18}O$ values (~−8 to ~−11‰) during deep glacial periods (~160 to ~135 ka and ~75 to ~20 ka), compared with more negative $\delta^{18}O$ values (~−11 to ~−15‰) during interglacial periods (~125 ka and after ~10 ka).

DISCUSSION

The CBoB speleothem $\delta^{18}O$ as a proxy of ISM rainfall

Our speleothem $\delta^{18}O$ variability is similar to the trends in speleothem records from the ISM domain (figs. S8 and S9) (*20*–*22*), as well as broadly consistent with the records from the East Asian summer monsoon (EASM) domain (figs. S9 and S10) (*1*, *2*), which, together with other lines of evidence (see Supplementary Text and table S2), suggests that the carbonate $\delta^{18}O$ in our samples primarily captured the rainfall $\delta^{18}O$ and cave temperature at the time of

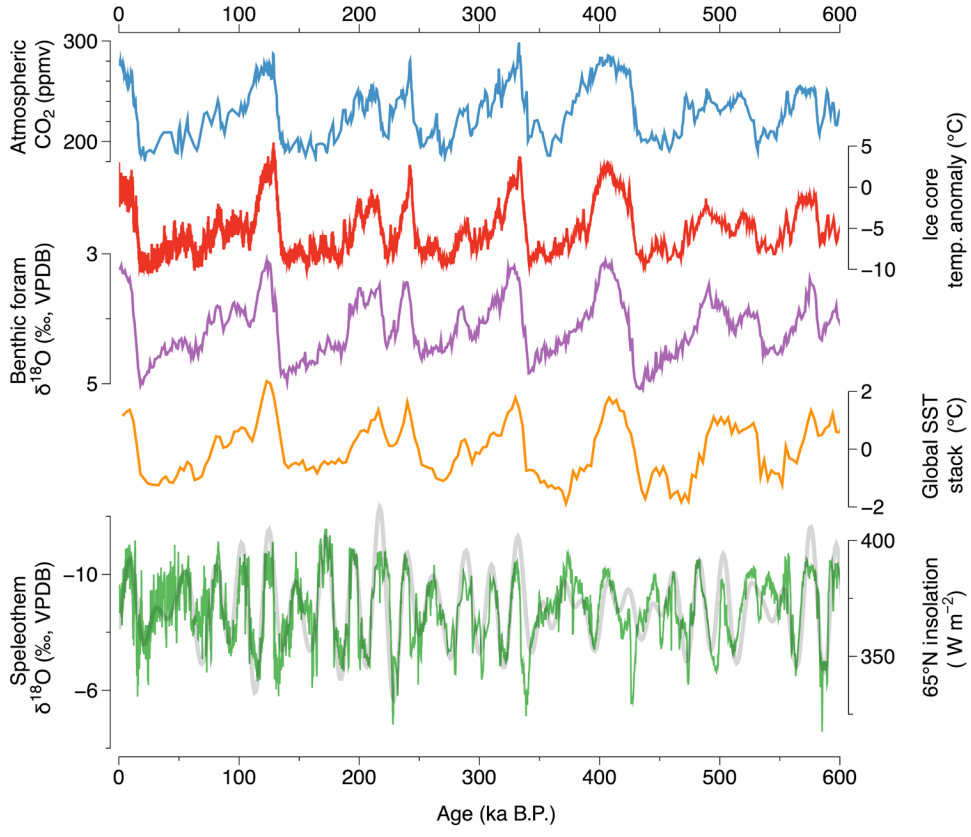

Fig. 1. Comparison of the Chinese speleothem $\delta^{18}O$ record and other major paleoclimate records. The compiled speleothem $\delta^{18}O$ record from southern China (green) (*2*) follows the 65°N summer insolation (gray) closely, and it is dominated by the 23-ka precessional cycle. However, variation in other major paleoclimate records, such as atmospheric CO_2 concentration (blue) (*6*) and Antarctica surface temperature anomaly (red) (*7*) retrieved from European Project for Ice Coring in Antarctica (EPICA) Dome C ice core, benthic foraminifera $\delta^{18}O$ LR04 stack (purple) (*8*), and global sea surface temperature (SST) stack (orange) (*9*), are dominated by the ~100-kyr glacial-interglacial cycle. VPDB, Vienna Pee Dee belemnite; B.P., before the present.

carbonate precipitation. In addition, as the temperature in the region likely fluctuated ~4° to 5°C during the recent glacial cycles (*23*, *24*), temperature-dependent fractionation accounts for only ~1.0‰ of the variability (*25*) in speleothem $\delta^{18}O$. A large portion of the variability in our samples must have resulted from changes in rainfall $\delta^{18}O$.

Rainfall $\delta^{18}O$ at our southern study site near the coastline is negligibly influenced by the continental effect and water recycling. $\delta^{18}O$ there is then primarily reflecting an isotope fractionation process close to that in the Rayleigh fractionation model. We, thus, argue that fluctuation of speleothem $\delta^{18}O$ at CBoB reflects AM rainfall or, more specifically, ISM rainfall.

The $\delta^{18}O$ fluctuation in our CBoB record closely matches the record from the Mawmluh Cave in northeastern India (fig. S8) (*21*, *26*), which is also located close to the BoB. We therefore combined the two records by negatively shifting $\delta^{18}O$ in the Mawmluh record by ~2.1‰ to account for their difference in cave temperature (fig. S8). The combined record shows broad similarity to various planktonic foraminiferal records from the BoB (*5*, *27*–*29*), in particular the foraminiferal *Globigerinoides ruber* $\delta^{18}O$ record from the northern BoB near the mouth of the Ganges-Brahmaputra rivers (Fig. 3 and fig. S1), which is also interpreted as fluvial input or ISM intensity (*27*). Hence, the resemblance further supports our interpretation of speleothem $\delta^{18}O$ as a proxy of ISM rainfall and, thus, its strength.

Reduced ISM rainfall during the LGM

The most prominent feature of the CBoB record is the 3.7‰ difference in $\delta^{18}O$ between the LGM and the recent several hundred years (Fig. 3, fig. S7A, and table S3)—one of the largest speleothem $\delta^{18}O$ differences in the AM region. A similar >3‰ difference is observable in the Mawmluh record (fig. S8) (*21*, *26*). If we consider a 0.7‰ change resulting from temperature effect on isotope fractionation during cave calcite precipitation (table S3), the speleothem $\delta^{18}O$ shifts in both records are in accordance with a >2‰ increase in groundwater $\delta^{18}O$ recovered in Bangladesh and dates back to the LGM (*30*). If we further consider a ~1‰ change in source seawater $\delta^{18}O$ resulting largely from ice volume changes (fig. S11) (*31*), the remaining shift of ~2‰ in the CBoB record, together with an up to 2‰ increase in the BoB ice-volume–corrected surface seawater $\delta^{18}O$ (*5*, *23*) during the LGM compared with the present, likely suggests a substantial decrease in monsoon rainfall amount during the LGM relative to the recent several hundred years.

We quantitatively estimate the reduction of rainfall amount using the Rayleigh distillation model, since the monsoonal moisture over the CBoB region comes dominantly from the tropical Indian Ocean, with almost no influence of the continental effect on rainfall $\delta^{18}O$. We assume that oxygen isotope exchanges remain in equilibrium state during water evaporation and condensation, and apply the

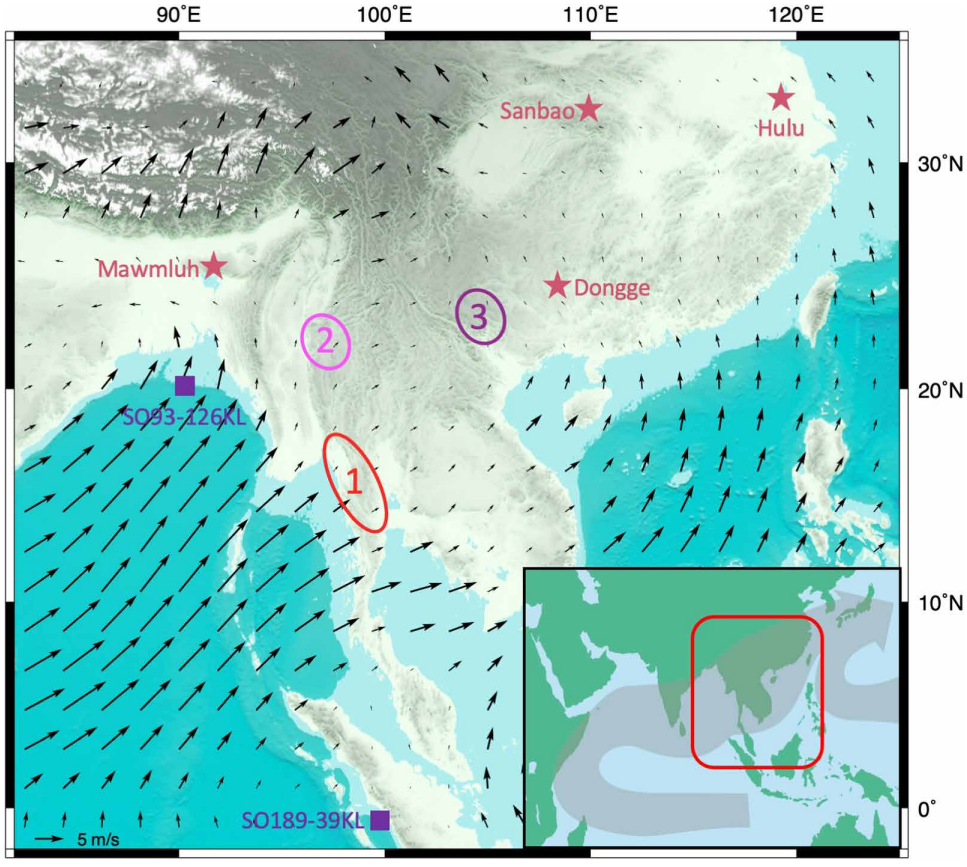

Fig. 2. Sample locations. The black arrows represent the present-day averaged June-July-August (JJA) wind pattern 10 m above sea level [data from the National Centers for Environmental Prediction/National Center for Atmospheric Research Reanalysis monthly mean (1981 to 2010) (*58*)]. The insert shows the AM system [modified after (*59*)]. The circled numbers mark the three strategic cave sites along the monsoon trajectory (1, CBoB; 2, CM; and 3, SEY). The stars mark the Mawmluh (*21*, *26*), Hulu (*60*), Dongge (*2*, *61*, *62*), and Sanbao (*1*, *2*) caves; and squares mark marine sediment cores SO93-126KL (*27*) and SO189-39KL (*39*) for reference.

following equation (*32*) to calculate the fraction of the original water vapor remaining in air masses (f)

$$(1000 + \delta^{18}O_p)/(1000 + \delta^{18}O_{sw}) = f^{(\alpha(\text{liquid-vapor})-1)} \quad (1)$$

where $\delta^{18}O_{sw}$ is seawater $\delta^{18}O$, $\delta^{18}O_p$ is the local precipitation $\delta^{18}O$, and α(liquid-vapor) is the isotopic fractionation factor between water liquid and vapor phases. $\delta^{18}O_{sw}$ is assigned to be 0‰ [VSMOW (Vienna standard mean ocean water)] for today and 1‰ during the LGM (*31*). We calculate $\delta^{18}O_p$ based on the equation

$$\alpha(\text{calcite-}H_2O) = (1000 + \delta^{18}O_c)/(1000 + \delta^{18}O_p) \quad (2)$$

where α(calcite-H_2O) is the isotopic fractionation factor between calcite and cave drip water and can be calculated from the equation (*25*)

$$1000 \times \ln\alpha(\text{calcite-}H_2O) = 17.66 \times 10^3/T - 30.16 \quad (3)$$

$\delta^{18}O_c$ is a calcite $\delta^{18}O$ value, read from the CBoB speleothem record. α(liquid-vapor) is the isotopic fractionation factor between water liquid and vapor phases, and we calculate it from the equation (*33*)

$$1000 \times \ln\alpha(\text{liquid-vapor}) = -7.685 + 6.7123 \times 10^3/T - 1.6664 \times 10^6/T^2 + 0.35041 \times 10^9/T^3 \quad (4)$$

where T is the temperature (in kelvin).

Assuming that the temperature at CBoB was ~4°C lower in the LGM relative to modern temperature (~28°C), in concert with the observed and simulated sea surface temperature (SST) drop in the BoB (*5*, *23*, *34*, *35*), our calculation shows that f changed from today's 54 to 68% during the LGM (table S3).

We then use the local precipitable water vapor (PWV; in kg/m^2 or mm) and the percentage of water vapor removed from air masses after reaching cave sites (i.e., $1 - f$) to calculate the precipitation amount at CBoB. We estimate PWV according to the equation (*36*)

$$\text{PWV} = 4932 \times \text{RH} \times e/T \quad (5)$$

where T is the temperature (in kelvin), RH is the relative humidity, and e is the saturation vapor pressure (in kPa), which we calculate from the equation (*37*)

$$e = 0.61121 \times e^{(17.368 \times Tc/(238.88+Tc))} \quad (6)$$

where Tc is the temperature (in Celsius). Given a relative humidity of 100%, we can estimate the moisture removed from air masses relative to the modern value (set as a reference point at 100%) (table S3).

On the basis of our calculations, the 3.7‰ difference in speleothem $\delta^{18}O$ between the LGM and the recent several hundred years

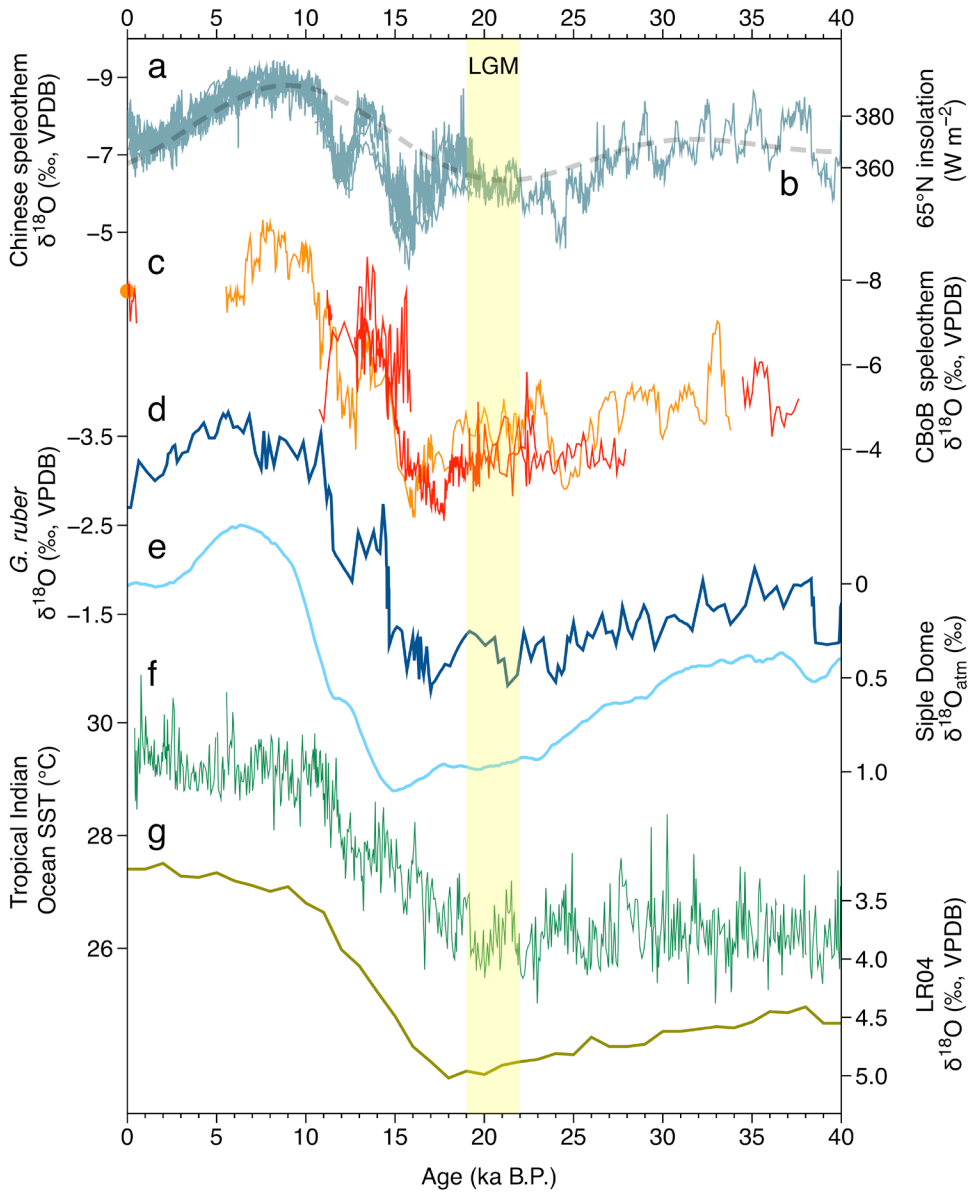

Fig. 3. Weakened ISM during the LGM and glacial boundary conditions. (**A**) The compiled speleothem $\delta^{18}O$ record from Hulu Cave (*2*, *60*), Dongge Cave (*61*, *62*), and Sanbao Cave, with the Sanbao record shifted positively by 1.6‰ to align it with the other two cave records from southern China (*1*). (**B**) The 65°N summer (JJA) insolation. (**C**) The combined speleothem records from CBoB (red) and Mawmluh (orange) (*21*, *26*) caves. The Mawmluh record is shifted negatively by 2.1‰ after correcting it for temperature effect on calcite $\delta^{18}O$, and the orange dot marks the mean value of a modern stalagmite (see the Supplementary Materials). (**D**) *G. ruber* $\delta^{18}O$ record, retrieved from sediment core SO93-126KL, as a proxy for ISM intensity (*27*). (**E**) Atmospheric molecular oxygen $\delta^{18}O$ record ($\delta^{18}O_{atm}$), retrieved from the Antarctica Siple Dome ice core (*38*). (**F**) Tropical Indian Ocean SST reconstructed from sediment core SO189-39KL (*39*). (**G**) Benthic foraminifera $\delta^{18}O$ LR04 stack (*8*).

suggests that ISM rainfall during the LGM decreased to about 56% of today's value (table S3). Not only is this value comparable to the ~58% calculated for the eastern Amazon lowlands (*32*), but together, these values also imply a much weakened hydrological cycle in the deep tropics when Earth was in a full glacial state and, hence, are consistent with an increase in $\delta^{18}O$ of atmospheric O_2 during the LGM (Fig. 3) (*38*).

The reduced ISM strength during the LGM is attributable mainly to a combination of a lower SST over the tropical Indian Ocean and a larger continental ice/snow coverage (Fig. 3). Tropical SST dropped by ~3°C (*23*, *39*), weakening convection over the region, decreasing rainfall, and increasing $\delta^{18}O$ values of precipitation over the ISM domain. Meanwhile, the ice/snow expansion on the continent increased albedo and reduced sensible heating (*35*, *40*); therefore, the expansion also weakened monsoonal rainfall. The exposure of the Sunda/Sahul shelf was shown by climate simulations as another key forcing of the tropical climate during the LGM, yet the same experiments were unable to capture large rainfall reduction in southern Myanmar (*35*).

Moisture transport pathway effect

The difference in $\delta^{18}O$ between the LGM and recent several hundred years decreases landward following the moisture trajectory, with ~2 and

<1‰ at CM and SEY, respectively (Fig. 4 and fig. S7, B and C). Since the NHSI values during the LGM were very close to those of today's, such a spatial-temporal pattern clearly shows that speleothem $\delta^{18}O$ is more sensitive to glacial forcings in coastal regions compared with those inland. We highlighted the spatial pattern by calculating the mean $\delta^{18}O$ values for every thousand years in each record and corrected locations other than CBoB for temperature effect (see Materials and Methods and fig. S11). The corrected records show a broad ^{18}O-depletion trend inlandward, consistent with the progressive rainout or Rayleigh distillation effect on water isotopes, implying a relatively stable trajectory of monsoon moisture for at least the recent ~40 ka (Fig. 4 and fig. S12). However, the offset between the records, which essentially describes the gradient of rainfall $\delta^{18}O$ across mainland Southeast Asia, was much larger (~8 to 10‰) during the last glacial period, particularly the LGM, compared with today or broadly the Holocene (~5 to 7‰), suggesting a stronger-than-today isotope fractionation of rainfall during the last glacial period (total difference ~3‰).

Following an early study (*41*), we term this change in isotope gradient through time the moisture transport pathway effect. We argue that the pathway effect reasonably explains the apparently different sensitivities of speleothem $\delta^{18}O$ to glacial forcings.

Changes in glacial forcings have led to a large negative shift in precipitation $\delta^{18}O$ between the LGM and the present, such as the >3‰ difference recorded in speleothems from the CBoB and Mawmluh caves. However, as a result of the pathway effect, the negative $\delta^{18}O$ shift becomes gradually muted inland, to as low as <1‰ at SEY. Underestimating this pathway effect could lead to inconsistent conclusions on the $\delta^{18}O$ sensitivities to climate forcings. For example, the CBoB $\delta^{18}O$ record suggests that glacial boundary conditions strongly forced the ISM (Fig. 3 and fig. S7A), while the SEY record (fig. S7C) implies a strong influence of the NHSI but insensitivity to glacial forcings, which is, in fact, similar to the characteristic Chinese records (fig. S9).

Mechanism for the pathway effect

What may have caused the pathway effect? Here, we propose that it is temperature, possibly together with suppressed plant transpiration.

During the last glacial period, the global temperature was much lower (by ~4°C or more) than today's, in particular on the continent, due to an enhanced ice albedo and lower atmospheric CO_2 (*10*, *42*), while the latitudinal temperature gradient was larger (*43*). The lower global temperature and larger temperature gradient led to a stronger-than-modern isotopic distillation and, hence, progressively lower $\delta^{18}O$ values of rainfall toward the ISM downstream.

To test how much temperature effect accounts for the observed $\delta^{18}O$ gradient changes, we calculate the approximate rainfall $\delta^{18}O$ gradient based on a temperature-dependent Rayleigh distillation model, largely following an early study (*44*). Regardless of any moisture

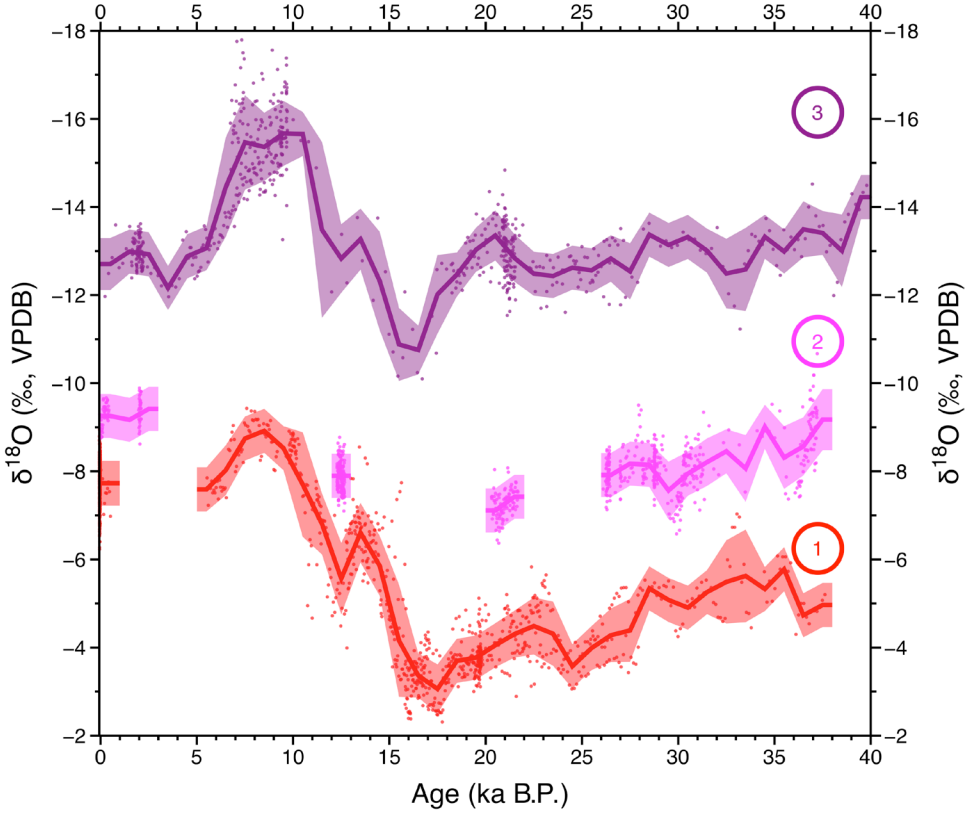

Fig. 4. Spatial-temporal comparison of speleothem $\delta^{18}O$ records from mainland Southeast Asia over the past 40 ka. The records obtained from the CBoB and Mawmluh (*21*, *26*) (site 1), CM (site 2), and SEY (site 3) caves are shown in red, pink, and purple, respectively. Note that the $\delta^{18}O$ in those records from locations other than CBoB has been corrected for temperature effect during calcite precipitation (see details in Materials and Methods). We further smoothed each record using 1000-year averages (thick lines). The shaded envelopes indicate the range of 1σ uncertainty of the $\delta^{18}O$ values. The comparison shows a broad ^{18}O-depletion trend from coastal sites to inland, associated with the progressive rainout effect on water isotopes. In addition, the isotopic gradient was larger during the LGM compared with today.

loss en route to CBoB, we assign the moisture remaining at CBoB as the initial state. We then calculate $\delta^{18}O$ of moisture and precipitation at SEY using the equation

$$(1000 + \delta^{18}O_v)/(1000 + \delta^{18}O_{vi}) = f^{(\alpha(\text{liquid-vapor})-1)} \quad (7)$$

where $\delta^{18}O_v$ is the remaining water vapor $\delta^{18}O$, and $\delta^{18}O_{vi}$ is its initial value, which we calculate with

$$(1000 + \delta^{18}O_{pi})/(1000 + \delta^{18}O_{vi}) = \alpha(\text{liquid-vapor}) \quad (8)$$

where $\delta^{18}O_{pi}$ is the speleothem inferred rainfall $\delta^{18}O$ at CBoB and can be read from table S3, α(liquid-vapor) is temperature dependent (Eq. 4), and *f* is the fraction of the initial water vapor remaining in air masses and is calculated by dividing PWV values (assuming RH = 100%) at different cave sites, which roughly decrease exponentially with temperature (Eqs. 5 and 6).

Applying the idealized Rayleigh distillation model, we find that the magnitudes of rainfall $\delta^{18}O$ decrease through the ISM transport trajectory are 6.0 and 7.7‰ for today and the LGM, respectively (fig. S13). Thus, temperature alone can explain ~1.7‰ out of the total ~3‰ difference in the $\delta^{18}O$ gradient between the LGM and the present across mainland Southeast Asia (Fig. 4).

We argue that the remaining ~1.3‰ results largely from changes in moisture recycling effect through suppressed plant transpiration but enhanced evaporation during the LGM. Different from evaporation, plant transpiration does not induce water isotope fractionation (*45*). Therefore, the proportion change of the two processes in moisture recycling can regulate the isotopic offset in rainfall between the last glacial period and the present (*32*). Various studies have indicated a reduction in forest coverage in now-heavily-forested Southeast Asia (*46*, *47*), which enhanced moisture recycling through evaporation but reduced plant transpiration during glacial periods, and likely also contributed to a steeper isotopic gradient in rainfall. Moisture transport by eddy diffusion is another physical process that influences the continental rainfall $\delta^{18}O$ gradient (*45*). For a given degree of rainout, eddy diffusion results in shallower gradients in precipitation isotopes. However, such influence in the humid tropics is rather weak (*45*).

The pathway effect in Chinese speleothem $\delta^{18}O$ records

The pathway effect, which in the end counteracts the forcing of glacial boundary conditions, is probably the key to the lack of glacial-interglacial variations in the inland speleothem $\delta^{18}O$ records. To further test our hypothesis, we compare speleothem $\delta^{18}O$ records from the ISM region with those from southern China (Fig. 5), where the records generally show weak glacial-interglacial variations. We focus specifically on MIS 5 and select three speleothem $\delta^{18}O$ records from sites broadly along the moisture pathway landward [i.e., SEY caves, Dongge Cave (*2*), and Sanbao Cave (*1*)]. Rainfall over southern China comes remotely from the tropical Indian Ocean by the ISM (*17*) or adjacently from the South China Sea and Western Pacific (*4*). The moisture from the latter source is isotopically heavier, which can lead to relatively higher $\delta^{18}O$ values in the Dongge and Sanbao cave records (*4*), thus explaining why the speleothems there do not record a landward ^{18}O-depletion trend.

Notable differences exist among the three cave records when comparing their amplitudes of $\delta^{18}O$ minima during MIS 5e (the last interglacial) to two subsequent interstadials MIS 5a and 5c: SEY $\delta^{18}O$ values were prominently the lowest during MIS 5e; Dongge

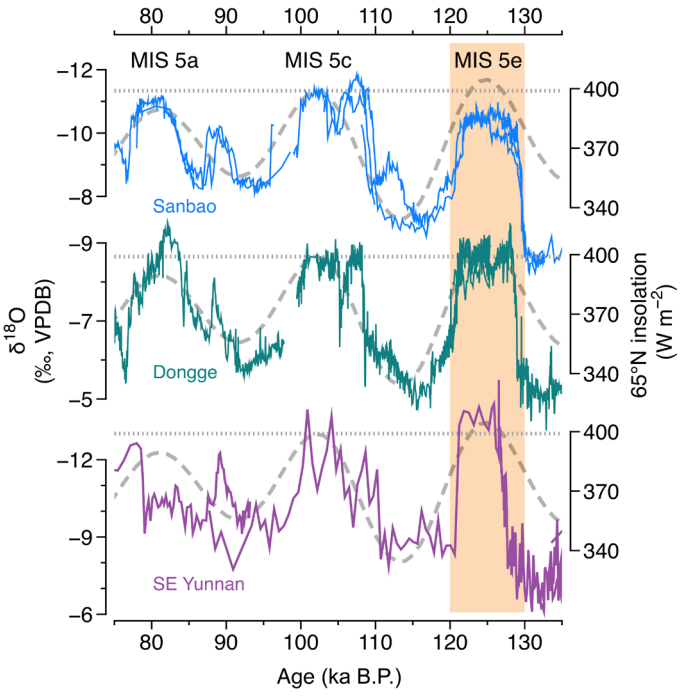

Fig. 5. Spatial-temporal comparison of speleothem $\delta^{18}O$ records from the SEY, Dongge (*2*) and Sanbao (*1*) caves in southern China during MIS 5. The summer (21 July) insolation at 65°N (the gray curve) is also plotted for comparison. To facilitate the comparison, we aligned the speleothem $\delta^{18}O$ values during MIS 5c with the insolation peak. The dashed lines, drawn from the MIS 5c insolation peak, indicate the difference among the three records in their amplitudes of $\delta^{18}O$ minima during MIS 5.

Cave $\delta^{18}O$ values during MIS 5e were similar to those during MIS 5a and 5c (*2*, *48*); and further inland, Sanbao Cave $\delta^{18}O$ values were the highest during MIS 5e (*1*). The $\delta^{18}O$ values during MIS5e in both Dongge and Sanbao records are clearly at odds not only with an enhanced insolation and stronger interglacial climate boundary conditions but also with the possibly reduced relative contribution of isotopically heavier moisture from the Pacific to the annual total precipitation (*20*). We hereby contend that the relatively positive $\delta^{18}O$ values in Dongge and, particularly, Sanbao speleothems can mainly be attributed to weakened isotopic distillation during MIS 5e, in line with the influence of the pathway effect. As the temperature differences among the three time periods are not prominent (*48*, *49*), the weakened isotopic distillation is possibly due to an enhanced plant transpiration effect during MIS 5e.

Our proposed moisture transport pathway effect reasonably explains the lack of glacial-interglacial variability in Chinese speleothem $\delta^{18}O$ records. During glacial periods, AM rainfall amount was significantly lower due to glacial climate boundary forcings, and meanwhile, transported moisture endured stronger isotope fractionation over the continent. In comparison, during interglacial periods, AM rainfall increased, but a weaker isotope fractionation of transported moisture led to apparently high speleothem $\delta^{18}O$ values in southern China.

MATERIALS AND METHODS

Cave settings and sample descriptions

We have analyzed 19 stalagmite samples from 11 different caves from three sites broadly located along the trajectory of the ISM (table S1).

While the climatology at our three sites differs, the overall rainfall in the region comes predominantly from the ISM (figs. S1 and S2). For example, although the annual rainfall varies from >2000 mm at CBoB to ~1000 mm at SEY, over 90% of the rainfall comes from the BoB and precipitates between late May and early November. The mean annual temperature is ~28°C at CBoB, dropping to ~15°C at SEY, largely due to combined latitudinal and altitudinal effects.

The CBoB contains four caves, including three in Mon State [Phabaung Gu (PHA)] and Kayin State [Padamya Gu (PDM) and Ya Thea Pyan Gu (YTP)], Myanmar, ~180 km to the southeast of Yangon, and one [Hin Tum No. 2 Cave (HT2)] in Uthai Thani province, Thailand, ~240 km to the northwest of Bangkok. The three Burmese caves, all located less than 100 m above sea level (asl), formed in tower karst, and the ages of the host carbonate rocks are unknown. The PHA (~1000 m long) and YTP (~400 m in length) caves contain multiple chambers. The PDM cave (~100 m long) has only one chamber but with a narrow entrance, which limits air ventilation. The HT2 cave (~200 m asl and ~300 m long) contains multiple chambers in argillaceous limestone that dates back to the Ordovician Period.

Our CM site includes the Lin Noe Twin (LNT) cave (~1300 m asl), located on the eastern side of the Shan Plateau. The cave formed within partially dolomitized Permian-Triassic limestone formations (*50*). The LNT cave consists of both an inner and an outer chamber. The outer chamber is small and narrow since its roof has collapsed; it also has a steep slope extending ~20 m downward. At its end, a narrow vertical drop of ~15 m leads to a large inner chamber, which is ~100 m in diameter and has poor ventilation.

In Yunnan, China, our six caves are located around 23.5°N, 104°E in Wenshan Prefecture (~2000 m asl), ~220 km to the southeast of Kunming. All SEY caves contain multiple chambers, likely longer than 1000 m.

To minimize the potential kinetic effect on carbonate stable isotope ratios, we only collected stalagmites from the inner chambers of the caves with very limited air ventilation and relative humidity close to 100%. All collected samples are made of calcite except for stalagmite A14, whose top 8 mm is calcite, while the rest is composed of aragonite. Moreover, in consideration of cave preservation, we almost exclusively collected broken stalagmites. The only standing stalagmite we collected was PHA02, with active dripping water. We used PHA02 to evaluate the equilibrium conditions of carbonate precipitation. Details about the caves, samples, and related regional climatology are in figs. S1 to S3 and table S1.

U-Th ages and stable isotopes

We halved all the stalagmites along the growth axes and polished their surfaces. We then drilled a total of 164 subsamples along the growth axes for ^{230}Th dating (fig. S4). We separated and purified uranium and thorium, following similar chemical procedures as described in (*51*) and (*52*) and analyzed all the CBoB, CM, and part of SEY samples in the Environmental Geochemistry Laboratory (EGL) at the Earth Observatory of Singapore (EOS)/Asian School of the Environment (ASE), Nanyang Technological University, Singapore, while we analyzed the remaining SEY samples at the Institute of Global Environmental Change (IGEC), Xi'an Jiaotong University, Xi'an, China. In both laboratories, the ^{230}Th dating techniques were identical, performed on Thermo-Finnigan Neptune Plus multi-collector inductively coupled plasma mass spectrometers using recently improved techniques (*18*, *19*).

We drilled a total of 2611 subsamples along the growth axes of the stalagmite samples at 1- to 10-mm increments for stable isotopic analysis (δ^{18}O and δ^{13}C) (figs. S5 and S6). We completed the measurements at three laboratories with different analytical systems: the EGL, EOS/ASE, Nanyang Technological University, Singapore; the Speleothem Isotope Laboratory (SIL), Nanjing Normal University, Nanjing, China; and the IGEC, Xi'an Jiaotong University, Xi'an, China. We report our results in per mil (‰), relative to the Vienna PeeDee Belemnite (VPDB) standard. At the EGL, we analyzed stable isotope samples using an online carbonate preparation system (Gasbench II) interfaced with a Thermo Fisher Scientific Delta V isotope ratio mass spectrometer (IRMS). We measured the stable isotope at the SIL on a Thermo-Finnigan MAT-253 IRMS equipped with a Kiel Carbonate Device III, and at the IGEC on a Thermo-Finnigan MAT-253 IRMS equipped with a Kiel Carbonate Device IV. At all the three laboratories, measurements of international carbonate standard NBS19 and in-house TTB1 standard showed a long-term reproducibility of ~0.1‰ or better (1σ). Cross-laboratory calibration confirms that stable isotope data are well reproduced among the three laboratories (e.g., fig. S5).

U and Th isotopic compositions and ^{230}Th dates are presented in data S1. ^{238}U concentrations range from 20 to 200 parts per billion (ppb), with a few exceptions (~3 to 13 parts per million) mainly in the aragonite portion of sample A14. ^{232}Th concentrations mostly range from fewer than 10 parts per trillion to the ppb level. We calculated ^{230}Th ages assuming an initial ^{230}Th/^{232}Th atomic ratio of $(4.4 \pm 2.2) \times 10^{-6}$, which is the value for a material at secular equilibrium, with the bulk Earth ^{232}Th/^{238}U value of 3.8. We considered it reasonable to adopt this value for initial ^{230}Th correction, as most samples had relatively high ^{230}Th/^{232}Th ratios, and initial correction was negligible. In addition, at the tip of modern stalagmite PHA02, ^{230}Th/^{232}Th atomic ratios are well within uncertainties of $(4.4 \pm 2.2) \times 10^{-6}$, which supports the assumption. The typical relative errors (2σ) in ages after the initial ^{230}Th correction for other samples are better than 1%, and all ^{230}Th dates are in stratigraphic order within 2σ errors, further confirming the data robustness (*53*). We used the StalAge method (*54*) to establish the chronology for samples with large errors in their age dating due to low U and high Th contents (e.g., HT2-1), or for samples whose ages have minor inversions (i.e., age inversions still within uncertainties, for example, XR05). We assumed that the top ~1 cm above a hiatus in sample PDM02 grew steadily between 11.2 and 11.5 ka. We used linear interpolation to establish the chronology for the rest of the samples (fig. S4).

The stable isotope (δ^{13}C and δ^{18}O) compositions are in data S2. δ^{18}O shows large shifts, ranging from −8.6 to −2.3‰, −9.0 to −4.7‰, and − 16.1 to −6.1‰ in the CBoB, CM, and SEY speleothem samples, respectively (figs. S5 to S7).

Rainfall δ^{18}O gradient across mainland Southeast Asia

Carbonate δ^{18}O in our samples reflected mostly the rainfall δ^{18}O and cave temperature at the time of carbonate precipitation. To better portray the spatial pattern of rainfall δ^{18}O, we corrected the speleothem calcite δ^{18}O values from sites other than the CBoB for temperature-dependent isotope fractionation resulting from the differences in cave temperatures. The modern cave temperatures are similar to the mean annual temperatures of nearby cities, that is, 28°C in the CBoB caves (near Yangon and Bangkok), 18°C in Mawmluh Cave (near Shillong), 20°C in CM LNT cave (near Taunggyi), and 15°C in SEY caves (near Kunming). We assumed

that the temperature differences among these caves have not changed through time.

The temperature differences among the cave sites were in fact likely larger during glacial periods, since the global meridional temperature gradient was generally larger (*43*) and the tropical lapse rate was possibly steeper (*55*, *56*). For example, during the LGM, the temperature likely dropped between 2° and 4°C at CBoB (*5*, *20*, *27*, *29*, *34*) and between 4° and 8°C at SEY (*20*, *24*, *57*). Model simulations also suggest an increase of ~2°C/1000 km in the regional temperature gradient during the LGM (*20*). Note that we considered here only the overall temperature gradient across mainland Southeast Asia from CBoB to SEY (~1000 km apart), as to date, we have only limited knowledge of the climatology of CM. An amplified temperature gradient during the LGM would have shifted speleothem $\delta^{18}O$ even more positively in the downwind region relative to local rainfall $\delta^{18}O$. Therefore, the aforementioned assumption provides a conservative estimate of the rainfall $\delta^{18}O$ gradient in our study area during the LGM. The rainfall $\delta^{18}O$ gradient was possibly larger than estimated here but would not have differed substantially because of the small temperature-dependent fractionation factor of oxygen isotopes between speleothem calcite and cave drip water (~−0.21‰/°C) (*25*).

After we remove site-specific temperature effect on speleothem $\delta^{18}O$ (figs. S8 and S11), the difference between the contemporaneous speleothem $\delta^{18}O$ values at CBoB and SEY is essentially equivalent to the difference in rainfall $\delta^{18}O$ values in the region (Fig. 4 and fig. S12B), as cave temperature effect and ocean reservoir effect in speleothem $\delta^{18}O$ through time cancel each other (*32*). The speleothem $\delta^{18}O$ gradient obtained by dividing the speleothem $\delta^{18}O$ offset by the length of the transect (~1000 km) is, therefore, a good approximation of the overall rainfall $\delta^{18}O$ gradient across the region following the monsoon trajectory. Again, we considered only the overall gradient across mainland Southeast Asia from the CBoB to SEY sites.

We further highlighted the spatial pattern by calculating the mean $\delta^{18}O$ values and their SDs for every 1000 years, assuming 0.5‰ as the minimum 1σ SD, as smaller SDs could also reflect relatively sparse data points. During the most recent 1000 years, the speleothem $\delta^{18}O$ values, after the site-specific temperature correction, have decreased by 5.2 ± 0.7‰ across mainland Southeast Asia (Fig. 4). This ~5.2‰/1000 km gradient reflects to a large extent the temperature gradient (~13°C/1000 km) across the transect, which is due to a combination of altitude and latitude effects. Our records show that the $\delta^{18}O$ gradient was much larger during the last glacial time (~8 to 10‰/1000 km or more if we consider the aforementioned amplified temperature effect) relative to today or broadly the Holocene (~5 to 7‰/1000 km), suggesting a stronger-than-today isotope fractionation of precipitation $\delta^{18}O$ during the last glacial period (total difference ~3‰) (Fig. 4).

SUPPLEMENTARY MATERIALS

Supplementary material for this article is available at http://advances.sciencemag.org/cgi/content/full/6/7/eaay8189/DC1

REFERENCES AND NOTES

1. Y. Wang, H. Cheng, R. L. Edwards, X. Kong, X. Shao, S. Chen, J. Wu, X. Jiang, X. Wang, Z. An, Millennial- and orbital-scale changes in the East Asian monsoon over the past 224,000 years. *Nature* **451**, 1090–1093 (2008).
2. H. Cheng, R. L. Edwards, A. Sinha, C. Spötl, L. Yi, S. Chen, M. Kelly, G. Kathayat, X. Wang, X. Li, X. Kong, Y. Wang, Y. Ning, H. Zhang, The Asian monsoon over the past 640,000 years and ice age terminations. *Nature* **534**, 640–646 (2016).
3. Z. An, G. Wu, J. Li, Y. Sun, Y. Liu, W. Zhou, Y. Cai, A. Duan, L. Li, J. Mao, H. Cheng, Z. Shi, L. Tan, H. Yan, H. Ao, H. Chang, J. Feng, Global monsoon dynamics and climate change. *Annu. Rev. Earth Planet. Sci.* **43**, 29–77 (2015).
4. S. C. Clemens, W. L. Prell, Y. Sun, Orbital-scale timing and mechanisms driving Late Pleistocene Indo-Asian summer monsoons: Reinterpreting cave speleothem $\delta^{18}O$. *Paleoceanography* **25**, PA4207 (2010).
5. D. Gebregiorgis, E. C. Hathorne, L. Giosan, S. Clemens, D. Nürnberg, M. Frank, Southern Hemisphere forcing of South Asian monsoon precipitation over the past ~1 million years. *Nat. Commun.* **9**, 4702 (2018).
6. D. Lüthi, M. Le Floch, B. Bereiter, T. Blunier, J.-M. Barnola, U. Siegenthaler, D. Raynaud, J. Jouzel, H. Fischer, K. Kawamura, T. F. Stocker, High-resolution carbon dioxide concentration record 650,000–800,000 years before present. *Nature* **453**, 379–382 (2008).
7. J. Jouzel, V. Masson-Delmotte, O. Cattani, G. Dreyfus, S. Falourd, G. Hoffmann, B. Minster, J. Nouet, J. M. Barnola, J. Chappellaz, H. Fischer, J. C. Gallet, S. Johnsen, M. Leuenberger, L. Loulergue, D. Luethi, H. Oerter, F. Parrenin, G. Raisbeck, D. Raynaud, A. Schilt, J. Schwander, E. Selmo, R. Souchez, R. Spahni, B. Stauffer, J. P. Steffensen, B. Stenni, T. F. Stocker, J. L. Tison, M. Werner, E. W. Wolff, Orbital and millennial antarctic climate variability over the past 800,000 years. *Science* **317**, 793–796 (2007).
8. L. E. Lisiecki, M. E. Raymo, A Pliocene-Pleistocene stack of 57 globally distributed benthic $\delta^{18}O$ records. *Paleoceanography* **20**, PA1003 (2005).
9. J. D. Shakun, D. W. Lea, L. E. Lisiecki, M. E. Raymo, An 800-kyr record of global surface ocean $\delta^{18}O$ and implications for ice volume-temperature coupling. *Earth Planet. Sci. Lett.* **426**, 58–68 (2015).
10. P. U. Clark, A. S. Dyke, J. D. Shakun, A. E. Carlson, J. Clark, B. Wohlfarth, J. X. Mitrovica, S. W. Hostetler, A. M. McCabe, The last glacial maximum. *Science* **325**, 710–714 (2009).
11. D. Yuan, H. Cheng, R. L. Edwards, C. A. Dykoski, M. J. Kelly, M. Zhang, J. Qing, Y. Lin, Y. Wang, J. Wu, J. A. Dorale, Z. An, Y. Cai, Timing, duration, and transitions of the last interglacial asian monsoon. *Science* **304**, 575–578 (2004).
12. F. S. R. Pausata, D. S. Battisti, K. H. Nisancioglu, C. M. Bitz, Chinese stalagmite $\delta^{18}O$ controlled by changes in the Indian monsoon during a simulated Heinrich event. *Nat. Geosci.* **4**, 474–480 (2011).
13. Z. Liu, X. Wen, E. C. Brady, B. Otto-Bliesner, G. Yu, H. Lu, H. Cheng, Y. Wang, W. Zheng, Y. Ding, R. L. Edwards, J. Cheng, W. Liu, H. Yang, Chinese cave records and the East Asia Summer Monsoon. *Quat. Sci. Rev.* **83**, 115–128 (2014).
14. J. W. Beck, W. Zhou, C. Li, Z. Wu, L. White, F. Xian, X. Kong, Z. An, A 550,000-year record of East Asian monsoon rainfall from ^{10}Be in loess. *Science* **360**, 877–881 (2018).
15. E. Huang, Y. Chen, E. Schefuß, S. Steinke, J. Liu, J. Tian, G. Martínez-Méndez, M. Mohtadi, Precession and glacial-cycle controls of monsoon precipitation isotope changes over East Asia during the Pleistocene. *Earth Planet. Sci. Lett.* **494**, 1–11 (2018).
16. B. Wang, S. C. Clemens, P. Liu, Contrasting the Indian and East Asian monsoons: Implications on geologic timescales. *Mar. Geol.* **201**, 5–21 (2003).
17. Y. Ding, J. C. L. Chan, The East Asian summer monsoon: An overview. *Meteorog. Atmos. Phys.* **89**, 117–142 (2005).
18. H. Cheng, L. R. Edwards, C.-C. Shen, V. J. Polyak, Y. Asmerom, J. Woodhead, J. Hellstrom, Y. Wang, X. Kong, C. Spötl, X. Wang, E. Calvin Alexander Jr., Improvements in ^{230}Th dating, ^{230}Th and ^{234}U half-life values, and U–Th isotopic measurements by multi-collector inductively coupled plasma mass spectrometry. *Earth Planet. Sci. Lett.* **371-372**, 82–91 (2013).

19. H.-W. Chiang, Y. Lu, X. Wang, K. Lin, X. Liu, Optimizing MC-ICP-MS with SEM protocols for determination of U and Th isotope ratios and ^{230}Th ages in carbonates. *Quat. Geochronol.* **50**, 75–90 (2019).
20. Y. Cai, I. Y. Fung, R. L. Edwards, Z. An, H. Cheng, J.-E. Lee, L. Tan, C.-C. Shen, X. Wang, J. A. Day, W. Zhou, M. J. Kelly, J. C. H. Chiang, Variability of stalagmite-inferred Indian monsoon precipitation over the past 252,000 y. *Proc. Natl. Acad. Sci. U.S.A.* **112**, 2954–2959 (2015).
21. S. Dutt, A. K. Gupta, S. C. Clemens, H. Cheng, R. K. Singh, G. Kathayat, R. L. Edwards, Abrupt changes in Indian summer monsoon strength during 33,800 to 5500 years B.P. *Geophys. Res. Lett.* **42**, 5526–5532 (2015).
22. G. Kathayat, H. Cheng, A. Sinha, C. Spötl, R. L. Edwards, H. Zhang, X. Li, L. Yi, Y. Ning, Y. Cai, W. L. Lui, S. F. M. Breitenbach, Indian monsoon variability on millennial-orbital timescales. *Sci. Rep.* **6**, 24374 (2016).
23. R. Saraswat, D. W. Lea, R. Nigam, A. Mackensen, D. K. Naik, Deglaciation in the tropical Indian Ocean driven by interplay between the regional monsoon and global teleconnections. *Earth Planet. Sci. Lett.* **375**, 166–175 (2013).
24. E. Zhang, J. Chang, J. Shulmeister, P. Langdon, W. Sun, Y. Cao, X. Yang, J. Shen, Summer temperature fluctuations in Southwestern China during the end of the LGM and the last deglaciation. *Earth Planet. Sci. Lett.* **509**, 78–87 (2019).
25. V. E. Johnston, A. Borsato, C. Spötl, S. Frisia, R. Miorandi, Stable isotopes in caves over altitudinal gradients: Fractionation behaviour and inferences for speleothem sensitivity to climate change. *Clim. Past* **9**, 99–118 (2013).
26. E. R. Ronay, S. F. M. Breitenbach, J. L. Oster, Sensitivity of speleothem records in the Indian Summer Monsoon region to dry season infiltration. *Sci. Rep.* **9**, 5091 (2019).
27. H. R. Kudrass, A. Hofmann, H. Doose, K. Emeis, H. Erlenkeuser, Modulation and amplification of climatic changes in the Northern Hemisphere by the Indian summer monsoon during the past 80 k.y. *Geology* **29**, 63–66 (2001).
28. P. Govil, P. Divakar Naidu, Variations of Indian monsoon precipitation during the last 32kyr reflected in the surface hydrography of the Western Bay of Bengal. *Quat. Sci. Rev.* **30**, 3871–3879 (2011).
29. D. Gebregiorgis, E. C. Hathorne, A. V. Sijinkumar, B. N. Nath, D. Nürnberg, M. Frank, South Asian summer monsoon variability during the last ~54 kyrs inferred from surface water salinity and river runoff proxies. *Quat. Sci. Rev.* **138**, 6–15 (2016).
30. P. K. Aggarwal, K. Fröhlich, K. M. Kulkarni, L. L. Gourcy, Stable isotope evidence for moisture sources in the asian summer monsoon under present and past climate regimes. *Geophys. Res. Lett.* **31**, L08203 (2004).
31. D. P. Schrag, J. F. Adkins, K. McIntyre, J. L. Alexander, D. A. Hodell, C. D. Charles, J. F. McManus, The oxygen isotopic composition of seawater during the Last Glacial Maximum. *Quat. Sci. Rev.* **21**, 331–342 (2002).
32. X. Wang, R. L. Edwards, A. S. Auler, H. Cheng, X. Kong, Y. Wang, F. W. Cruz, J. A. Dorale, H.-W. Chiang, Hydroclimate changes across the Amazon lowlands over the past 45,000 years. *Nature* **541**, 204–207 (2017).
33. J. Horita, D. J. Wesolowski, Liquid-vapor fractionation of oxygen and hydrogen isotopes of water from the freezing to the critical temperature. *Geochim. Cosmochim. Acta* **58**, 3425–3437 (1994).
34. H. Rashid, B. P. Flower, R. Z. Poore, T. M. Quinn, A ~25ka Indian Ocean monsoon variability record from the Andaman Sea. *Quat. Sci. Rev.* **26**, 2586–2597 (2007).
35. P. N. DiNezio, J. E. Tierney, B. L. Otto-Bliesner, A. Timmermann, T. Bhattacharya, N. Rosenbloom, E. Brady, Glacial changes in tropical climate amplified by the Indian Ocean. *Sci. Adv.* **4**, eaat9658 (2018).
36. B. Leckner, The spectral distribution of solar radiation at the earth's surface—elements of a model. *Sol. Energy* **20**, 143–150 (1978).
37. A. L. Buck, New equations for computing vapor pressure and enhancement factor. *J. Appl. Meteorol.* **20**, 1527–1532 (1981).
38. J. P. Severinghaus, R. Beaudette, M. A. Headly, K. Taylor, E. J. Brook, Oxygen-18 of O_2 records the impact of abrupt climate change on the terrestrial biosphere. *Science* **324**, 1431–1434 (2009).
39. M. Mohtadi, M. Prange, D. W. Oppo, R. De Pol-Holz, U. Merkel, X. Zhang, S. Steinke, A. Lückge, North Atlantic forcing of tropical Indian Ocean climate. *Nature* **509**, 76–80 (2014).
40. T. P. Barnett, L. Dumenil, U. Schlese, E. Roeckner, The effect of Eurasian snow cover on global climate. *Science* **239**, 504–507 (1988).
41. C. Hu, G. M. Henderson, J. Huang, S. Xie, Y. Sun, K. R. Johnson, Quantification of Holocene Asian monsoon rainfall from spatially separated cave records. *Earth Planet. Sci. Lett.* **266**, 221–232 (2008).
42. J. D. Shakun, P. U. Clark, F. He, S. A. Marcott, A. C. Mix, Z. Liu, B. Otto-Bliesner, A. Schmittner, E. Bard, Global warming preceded by increasing carbon dioxide concentrations during the last deglaciation. *Nature* **484**, 49–54 (2012).
43. S. Jasechko, A. Lechler, F. S. R. Pausata, P. J. Fawcett, T. Gleeson, D. I. Cendón, J. Galewsky, A. N. LeGrande, C. Risi, Z. D. Sharp, J. M. Welker, M. Werner, K. Yoshimura, Late-glacial to late-Holocene shifts in global precipitation δ^{18}O. *Clim. Past* **11**, 1375–1393 (2015).
44. E. A. Boyle, Cool tropical temperatures shift the global δ^{18}O-T relationship: An explanation for the ice core δ^{18}O-borehole thermometry conflict? *Geophys. Res. Lett.* **24**, 273–276 (1997).
45. M. J. Winnick, C. P. Chamberlain, J. K. Caves, J. M. Welker, Quantifying the isotopic "continental effect". *Earth Planet. Sci. Lett.* **406**, 123–133 (2014).
46. C. M. Wurster, M. I. Bird, I. D. Bull, F. Creed, C. Bryant, J. A. J. Dungait, V. Paz, Forest contraction in north equatorial Southeast Asia during the Last Glacial Period. *Proc. Natl. Acad. Sci. U.S.A.* **107**, 15508–15511 (2010).
47. Z. Cheng, C. Weng, S. Steinke, M. Mohtadi, Anthropogenic modification of vegetated landscapes in southern China from 6,000 years ago. *Nat. Geosci.* **194**, 1121 (2018).
48. T. Caley, D. M. Roche, H. Renssen, Orbital Asian summer monsoon dynamics revealed using an isotope-enabled global climate model. *Nat. Commun.* **5**, 5371 (2014).
49. F. Peterse, A. Martínez-García, B. Zhou, C. J. Beets, M. A. Prins, H. Zheng, T. I. Eglinton, Molecular records of continental air temperature and monsoon precipitation variability in East Asia spanning the past 130,000 years. *Quat. Sci. Rev.* **83**, 76–82 (2014).
50. T. Oo, T. Hlaing, N. Htay, Permian of Myanmar. *J. Asian Earth Sci.* **20**, 683–689 (2002).
51. L. R. Edwards, J. H. Chen, G. J. Wasserburg, ^{238}U-^{234}-U^{230}-Th^{232}-Th systematics and the precise measurement of time over the past 500,000 years. *Earth Planet. Sci. Lett.* **81**, 175–192 (1987).
52. H. Cheng, R. L. Edwards, J. Hoff, C. D. Gallup, D. A. Richards, Y. Asmerom, The half-lives of uranium-234 and thorium-230. *Chem. Geol.* **169**, 17–33 (2000).
53. J. Hellstrom, M. McCulloch, J. Stone, A detailed 31,000-year record of climate and vegetation change, from the isotope geochemistry of two New Zealand speleothems. *Quat. Res.* **50**, 167–178 (1998).
54. D. Scholz, D. L. Hoffmann, StalAge–An algorithm designed for construction of speleothem age models. *Quat. Geochronol.* **6**, 369–382 (2011).
55. A. K. Tripati, S. Sahany, D. Pittman, R. A. Eagle, J. D. Neelin, J. L. Mitchell, L. Beaufort, Modern and glacial tropical snowlines controlled by sea surface temperature and atmospheric mixing. *Nat. Geosci.* **7**, 205–209 (2014).
56. S. E. Loomis, J. M. Russell, D. Verschuren, C. Morrill, G. De Cort, J. S. Sinninghe Damsté, D. Olago, H. Eggermont, F. A. Street-Perrott, M. A. Kelly, The tropical lapse rate steepened during the Last Glacial Maximum. *Sci. Adv.* **3**, e1600815 (2017).
57. C. G. Cook, R. T. Jones, P. G. Langdon, M. J. Leng, E. Zhang, New insights on Late Quaternary Asian palaeomonsoon variability and the timing of the Last Glacial Maximum in southwestern China. *Quat. Sci. Rev.* **30**, 808–820 (2011).
58. E. Kalnay, M. Kanamitsu, R. Kistler, W. Collins, D. Deaven, L. Gandin, M. Iredell, S. Saha, G. White, J. Woollen, Y. Zhu, M. Chelliah, W. Ebisuzaki, W. Higgins, J. Janowiak, K. C. Mo, C. Ropelewski, J. Wang, A. Leetmaa, R. Reynolds, R. Jenne, D. Joseph, The NCEP/NCAR 40-year reanalysis project. *Bull. Am. Meteorol. Soc.* **77**, 437–471 (1996).
59. K. R. Johnson, Long-distance relationship. *Nat. Geosci.* **4**, 426–427 (2011).
60. Y. J. Wang, H. Cheng, R. L. Edwards, Z. S. An, J. Y. Wu, C.-C. Shen, J. A. Dorale, A high-resolution absolute-dated late pleistocene monsoon record from hulu cave, china. *Science* **294**, 2345–2348 (2001).
61. Y. Wang, H. Cheng, R. L. Edwards, Y. He, X. Kong, Z. An, J. Wu, M. J. Kelly, C. A. Dykoski, X. Li, The holocene asian monsoon: Links to solar changes and north atlantic climate. *Science* **308**, 854–857 (2005).
62. C. A. Dykoski, R. L. Edwards, H. Cheng, D. Yuan, Y. Cai, M. Zhang, Y. Lin, J. Qing, Z. An, J. Revenaugh, A high-resolution, absolute-dated Holocene and deglacial Asian monsoon record from Dongge Cave, China. *Earth Planet. Sci. Lett.* **233**, 71–86 (2005).
63. C. H. Hendy, The isotopic geochemistry of speleothems—I. The calculation of the effects of different modes of formation on the isotopic composition of speleothems and their applicability as palaeoclimatic indicators. *Geochim. Cosmochim. Acta* **35**, 801–824 (1971).
64. K. Yoshimura, T. Oki, S. Kanae, A quantitative analysis of short-term ^{18}O variability with a Rayleigh-type isotope circulation model. *J. Geophys. Res.* **108**, 1130 (2003).
65. G. J. Bowen, Isoscapes: Spatial pattern in isotopic biogeochemistry. *Annu. Rev. Earth Planet. Sci.* **38**, 161–187 (2010).
66. H. Cheng, R. L. Edwards, Y. Wang, X. Kong, Y. Ming, M. J. Kelly, X. Wang, C. D. Gallup, W. Liu, A penultimate glacial monsoon record from Hulu Cave and two-phase glacial terminations. *Geology* **34**, 217–220 (2006).
67. J. A. Dorale, R. L. Edwards, E. Ito, L. A. Gonzalez, Climate and vegetation history of the midcontinent from 75 to 25 ka: A Speleothem record from crevice cave, Missouri, USA. *Science* **282**, 1871–1874 (1998).
68. S.-T. Kim, J. R. O'Neil, Equilibrium and nonequilibrium oxygen isotope effects in synthetic carbonates. *Geochim. Cosmochim. Acta* **61**, 3461–3475 (1997).
69. S.-T. Kim, J. R. O'Neil, C. Hillaire-Marcel, A. Mucci, Oxygen isotope fractionation between synthetic aragonite and water: Influence of temperature and Mg^{2+} concentration. *Geochim. Cosmochim. Acta* **71**, 4704–4715 (2007).
70. C. Risi, A. Landais, R. Winkler, F. Vimeux, Can we determine what controls the spatio-temporal distribution of d-excess and ^{17}O-excess in precipitation using the LMDZ general circulation model? *Clim. Past* **9**, 2173–2193 (2013).
71. L. Merlivat, J. Jouzel, Global climatic interpretation of the deuterium-oxygen 18 relationship for precipitation. *J. Geophys. Res.* **84**, 5029–5033 (1979).

72. J. Jouzel, L. Merlivat, C. Lorius, Deuterium excess in an East Antarctic ice core suggests higher relative humidity at the oceanic surface during the last glacial maximum. *Nature* **299**, 688–691 (1982).
73. J. R. Gat, Oxygen and hydrogen isotopes in the hydrologic cycle. *Annu. Rev. Earth Planet. Sci.* **24**, 225–262 (1996).
74. M. Benetti, G. Reverdin, C. Pierre, L. Merlivat, C. Risi, H. C. Steen-Larsen, F. Vimeux, Deuterium excess in marine water vapor: Dependency on relative humidity and surface wind speed during evaporation. *J. Geophys. Res. Atmos.* **119**, 584–593 (2014).
75. M. Werner, B. Haese, X. Xu, X. Zhang, M. Butzin, G. Lohmann, Glacial–interglacial changes in $H_2{}^{18}O$, HDO and deuterium excess–results from the fully coupled ECHAM5/MPI-OM Earth system model. *Geosci. Model Dev.* **9**, 647–670 (2016).
76. R. Gonfiantini, The terrestrial environment, in *Handbook of Environmental Isotope Geochemistry*, B. P. Fritz, J. C. Fontes, Eds. (Elsevier, 1986), pp. 113–168.
77. F. Alshawaf, F. Zus, K. Balidakis, Z. Deng, M. Hoseini, G. Dick, J. Wickert, On the statistical significance of climatic trends estimated From GPS tropospheric time series. *J. Geophys. Res. Atmos.* **123**, 10967–10990 (2018).
78. K. Balidakis, T. Nilsson, F. Zus, S. Glaser, R. Heinkelmann, Z. Deng, H. Schuh, Estimating integrated water vapor trends from VLBI, GPS, and numerical weather models: Sensitivity to tropospheric parameterization. *J. Geophys. Res. Atmos.* **123**, 6356–6372 (2018).
79. J. Wang, Z. Wu, M. Semmling, F. Zus, S. Gerland, M. Ramatschi, M. Ge, J. Wickert, H. Schuh, Retrieving precipitable water vapor from shipborne multi-GNSS observations. *Geophys. Res. Lett.* **46**, 5000–5008 (2019).
80. C. H. Reitan, Surface dew point and water vapor aloft. *J. Appl. Meteorol.* **2**, 776–779 (1963).
81. F. Besharat, A. A. Dehghan, A. R. Faghih, Empirical models for estimating global solar radiation: A review and case study. *Renew. Sust. Energ. Rev.* **21**, 798–821 (2013).
82. M. G. Lawrence, The relationship between relative humidity and the dewpoint temperature in moist air: A simple conversion and applications. *Bull. Am. Meteorol. Soc.* **86**, 225–234 (2005).
83. F. J. Wentz, L. Ricciardulli, K. Hilburn, C. Mears, How much more rain will global warming bring? *Science* **317**, 233–235 (2007).
84. W. S. Broecker, Mountain glaciers: Recorders of atmospheric water vapor content? *Glob. Biogeochem. Cycles* **11**, 589–597 (1997).
85. H. Cheng, R. L. Edwards, W. S. Broecker, G. H. Denton, X. Kong, Y. Wang, R. Zhang, X. Wang, Ice age terminations. *Science* **326**, 248–252 (2009).
86. J. R. Petit, J. Jouzel, D. Raynaud, N. I. Barkov, J. M. Barnola, I. Basile, M. Bender, J. Chappellaz, M. Davis, G. Delaygue, M. Delmotte, V. M. Kotlyakov, M. Legrand, V. Y. Lipenkov, C. Lorius, L. PÉpin, C. Ritz, E. Saltzman, M. Stievenard, Climate and atmospheric history of the past 420,000 years from the Vostok ice core, Antarctica. *Nature* **399**, 429–436 (1999).
87. R. Bintanja, R. S. W. van de Wal, J. Oerlemans, Modelled atmospheric temperatures and global sea levels over the past million years. *Nature* **437**, 125–128 (2005).
88. M. Li, L. Hinnov, L. Kump, Acycle: Time-series analysis software for paleoclimate research and education. *Comput. Geosci.* **127**, 12–22 (2019).
89. I. Clark, P. Fritz, *Environmental Isotopes in Hydrogeology* (CRC Press, ed. 2, 1997).
90. S. Jasechko, Z. D. Sharp, J. J. Gibson, S. J. Birks, Y. Yi, P. J. Fawcett, Terrestrial water fluxes dominated by transpiration. *Nature* **496**, 347–350 (2013).
91. S. P. Good, D. Noone, G. Bowen, Hydrologic connectivity constrains partitioning of global terrestrial water fluxes. *Science* **349**, 175–177 (2015).

Acknowledgments: X.W. would like to thank W. Broecker, wherever he may be, for inspiration and support over the years. X.W. also thanks K. Sieh and Y. Wang for the introduction to fieldwork in Myanmar. We thank X. Kong and Z. Zhang for the help in the stable isotope measurements, and J. Severinghaus for sharing ice core $\delta^{18}O$ of the O_2 data. We thank the Tonongto family for fieldwork in Thailand. We acknowledge colleagues from Myanmar Geoscience Society and the local people in Myanmar, Thailand, and Yunnan, China, for help in field sampling. Special thanks to P. Adamek for help on the English editing of this manuscript. **Funding:** This work was funded by the National Research Foundation of Singapore under its NRF Fellowship scheme (award no. NRF-NRFF2011-08 to X.W.), the EOS, the National Research Foundation and the Singapore Ministry of Education under the Research Centers of Excellence initiative, an NSFC grant (no. 41888101 to H.-W.C.), an NRF-NSFC joint grant (no. NRF2017NRF-NSFC001-047 to X.W.), and a DPST research grant (award no. 042/2558 to S.C.). **Author contributions:** X.W. designed the project. X.W., G.L., X.L., H.-W.C., H.C., S.C., L.T.A., P.M.M., W.N.T., and K.M.O. performed the fieldwork and sampling. G.L., X.L., H.-W.C., S.Y., S.H., Y.L., X.W., and H.C. carried out the uranium/thorium dating and oxygen isotope measurements. G.L. and X.W. wrote the manuscript. All the authors discussed the results and implications and commented on the manuscript. **Competing interests:** The authors declare that they have no competing interests. **Data and materials availability:** All data needed to evaluate the conclusions in the paper are present in the paper and/or the Supplementary Materials. Additional data related to this paper may be requested from the authors.

Submitted 20 July 2019
Accepted 25 November 2019
Published 12 February 2020
10.1126/sciadv.aay8189

Citation: G. Liu, X. Li, H.-W. Chiang, H. Cheng, S. Yuan, S. Chawchai, S. He, Y. Lu, L. T. Aung, P. M. Maung, W. N. Tun, K. M. Oo, X. Wang, On the glacial-interglacial variability of the Asian monsoon in speleothem $\delta^{18}O$ records. *Sci. Adv.* **6**, eaay8189 (2020).